Using Divertor Strike Point Splitting to Understand Plasma Response and its Sensitivity Equilibrium Uncertainty

By
Abraham Teklu

A THESIS

submitted to

Oregon State University

University Honors College

in partial fulfillment of
the requirements for the
degree of

Honors Baccalaureate of Science in Physics
(Honors Scholar)

Presented May 24th, 2018
Commencement June 2018

AN ABSTRACT OF THE THESIS OF

Abraham Teklu for the degree of Honors Baccalaureate of Science in Physics
presented on May 24th, 2018. Title:
Using Divertor Strike Point Splitting to Understand Plasma Response and its Sensitivity Equilibrium

Abstract approved:

Heidi Schellman

Soon the largest fusion project in the world, ITER, will attempt to produce more fusion power than required to sustain the fusion reaction, this is known as ignition. The tokamak (a toroidal fusion device) being built in France will be running at such high temperatures that heat distribution is a problem. To prevent future calamity a tokamak run by General Atomics, DIII-D, is running experiments to modify the heat distribution in the divertor region; a narrow area on the floor of the tokamak. The resonant magnetic perturbations (RMPs) from 3D coils are varied to modify the splitting of the divertor strike points in DIII-D. This splitting is imaged in filtered visible and infrared emission to determine the particle and heat flux patterns on the target plates. The observed splitting is compared to vacuum modeling in discharges where a subset of the RMP coils were ramped to shift the divertor footprints from dominantly n = 3 to n = 2 pattern. The measured splitting has a very similar pattern to the modeled splitting, but is on a scale that is 5 times larger. These results could later be used to determine if the plasma response model can be validated with the measured splitting seen in the camera data. The sensitivity of the modeled splitting depend on details of the 2D equilibrium. The sequence of kinetic equilibria reproduce the time dependence of the measured splitting better than with magnetics only EFITs, indicating that the splitting is sensitive to aspects of the equilibria, such as the bootstrap current and q profile, that vary slowing during the discharge and aren't modeled in a magnetics only EFIT reconstruction. This RMP ramp technique could be used in ITER to spread out the heat flux while avoiding excessive forces on the RMP coils.

Key Words: Divertor, Splitting, Footprint, RMP

Corresponding e-mail address: teklua@oregonstate.edu

Using Divertor Strike Point Splitting to Understand Plasma Response and its Sensitivity Equilibrium Uncertainty

By
Abraham Teklu

A THESIS

submitted to

Oregon State University

University Honors College

in partial fulfillment of
the requirements for the
degree of

Honors Baccalaureate of Science in Physics
(Honors Scholar)

Presented May 24th, 2018
Commencement June 2018

Honors Baccalaureate of Science in Physics project of Abraham Teklu presented on May 24th, 2018

APPROVED:

Heidi Schellman, Mentor, representing Physics

Matthew Graham, Committee Member, representing Physics

Elizabeth Gire, Committee Member, representing Physics

Toni Doolen, Dean, Oregon State University Honors College

I understand that my project will become part of the permanent collection of Oregon State University Honors College. My signature below authorizes release of my project to any reader upon request.

Abraham Teklu, Author

Acknowledgements

Contributers
D.M. Orlov, R.A. Moyer, I. Bykov, *UCSD*
T.E. Evans, W. Wu, G.L. Trevisan, B.C. Lyons, T. Abrams, *General Atomics*
M.A. Makowski, C.S. Lasnier, M.E. Fenstermacher, *LLNL*

This research could not have been done without the help of Richard Moyer, Todd Evans, and Dmitri Orlov. As well as support from the Department of Energy through the SULI program. Many thanks to all of the contributers as well, especially Gregorio Trevisan, Igor Bykov, and Wen Wu who worked with me one on one to solve coding issues many times. *Work supported by U.S. DOE under the Science Undergraduate Laboratory Internship (SULI) program and DE-FC02-04ER54698, DE-FG02-07ER54917, DE-FG02-05ER54809 and DE-AC52-07NA2734

Contents

List of Figures

I Introduction

I.1 Motivation from Abroad

Energy sources have always been needed and soon the largest fusion project in the world, ITER, will be attempting to produce more fusion power than required to sustain the fusion reaction, this is known as ignition. The ITER tokamak (a toroidal fusion device) being built in France will be running at such high temperatures that heat distribution is a problem. Currently, edge localized modes - spurts from the edge of the plasma - aren't damaging to tokamaks, but are predicted to do significant damage in ITER. ELMs are controlled with resonant magnetic perturbations (RMPs). However, RMPs cause the ejected plasma to travel along open magnetic field lines in the tokamak and deposit plasma in the lower wall, also known as the divertor region [4]. Predictably modeling plasma footprint patterns will be an important step toward understanding how resonant magnetic perturbations effect magnetic fields in the plasma. This is the main goal of the DIII-D tokamak experiments presented here. Accurately predicting how the plasma responds in the divertor region will also support methods to spread the heat flux. This is of good consequence for ITER, when in normal operations, edge localized modes are expected to release $20 - 30$ MJ of energy into ITER [5].

I.2 Background

I.2.1 Tokamaks - Nuclear Fusion on Earth

For 60+ years fusion energy has been sought after by physicists. Now there are many types of fusion devices all over the world, but the most popular fusion device is the Tokamak. This fusion device relies on toroidal magnetic confinement to contain plasma at high enough temperatures (10 keV/k_B or 10^8 ^{o}C) to induce fusion, this is thermonuclear fusion. The fuel most commonly used in Tokamaks is deuterium and tritium, or D and T respectively. These isotopes of hydrogen, H^2 (D) and H^3 (T), undergo fusion to produce 17.6 MeV per reaction. A 3.5 MeV α particle is released and 14.1 MeV neutron is released during this reaction. D–T fuel is used because it has the highest reaction cross-section at the lowest ion energy. This helps sustain fusion at lower temperatures. Other ion combinations either reach their maximum cross-section at higher energies, have a smaller cross-section, or produce energy not as easily captured as a high energy neutron [1]. The neutron escapes magnetic confinement to strike a lithium blanket. This neutron lithium reaction produces tritium, fuel to keep the fusion reaction going, and also heats the blanket. The lithium blanket is cooled by a fluid and the heat from the fluid is converted to electrical power [6]. To give a sense of scale 1 g of D–T fuel could produce 10^5 kWh of energy [1].

Ignition is the point where the D–T reaction can sufficiently heat itself through

the α particles released in the reaction to sustain adequate temperatures for fusion. If the temperature or density drops too low the ions won't be able to overcome the Coulombic repulsion in a reasonable amount of time. These 3 factors - temperature, density, and time - are the deciding factors in ignition and when combined create a single criterion known as the fusion triple product.

$$nT\tau_E > 3 \times 10^{21} \mathrm{m}^{-3} \mathrm{keVs}[1] \tag{1}$$

In equation 1 n represents the fuel ion density in ions per meter cubed, T represents temperature in keV, and τ_E represents confinement time in seconds. This is the inequality plasma physicists have been fighting for the last 60+ years. In the past fusion devices were closer to the square root of the fusion triple product than ignition, but now fusion devices are nearing the same order of magnitude as the criterion.However, each step in higher density and temperature increases the plasma β, the plasma pressure over the magnetic field pressure. As β is increased, stability limits are exceeded leading to instabilities that can lead to either lose of confinement through increased plasma transport or sudden catastrophic loss of confinement via a nonlinearly bursting instability such as an ELM or a disruption that terminates the discharge.

The following images are excerpts from John Wesson's book Tokamaks. They are an ample descriptions of plasma in a tokamak. Notice the diagram in figure I.1 doesn't show any external components. The fields are generated from external components but everything in the diagram is contained within the plasma. Figures I.2 and I.3 display the external components that create the toroidal magnetic field and the plasma current. What creates the poloidal magnetic field is the plasma current itself.

I.2.2 Flux Surfaces and MHD Equilibrium

With all these magnetic fields and currents that exist within the tokamak, equilibrium has become quite complicated. Looking at the toroidal cross section in figure I.4 the plasma pressure exerts an outward force. In a straight cylinder, adding an axial magnetic field, analogous to $B\phi$ in a torus, causes the charged particles to gyrate around the magnetic field lines due to the Lorenz force. This provides for a low level of classical plasma confinement over no magnetic field in which the charged particles would diffuse down pressure gradients just like an ideal gas, and be unconfined. The term "classical" means due to collisions; in such a straight cylinder with some confinement, there will be a higher density on axis than at the edge; this means that across the cylinder, there will be more charged particles gyrating to larger minor radius than to smaller minor radius. Each time they collide they can jump to a new field line. Due to the asymmetry in the numbers of gyrating to larger minor radius vs. smaller minor radius, this produced a net diffusion of charged particles across

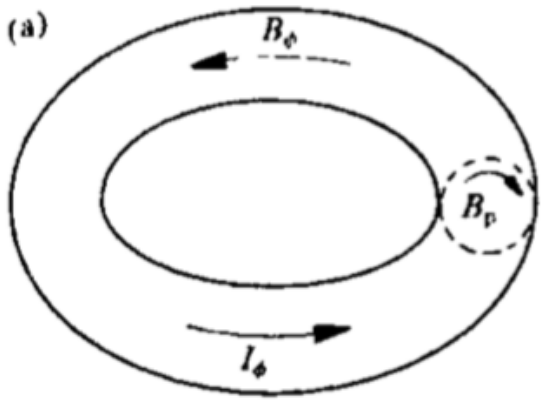

Figure I.1: This is a toroidally confined plasma with arrows displaying the toroidal magnetic field B_ϕ and the poloidal magnetic field B_θ. It is also showing the toroidal current I_ϕ, also known as the plasma current because it is the motion of the electrons; the plasma current creates the poloidal magnetic field. Note that the ions are so much more massive that the essentially don't move, don't carry the current.[1].

the axial magnetic field. However, even with this axial magnetic field, the plasma is still free to run out the ends of the cylinder because the axial magnetic field can only exert a force on the charged particles perpendicular to the B field.

Now, bend the cylinder into a torus; this stops the end losses but it turns out that a plasma confined in a torus with a purely axial (toroidal) B field can't be confined because the ions and electrons drift to the top and bottom of the torus, inducing an electric field that together with the B field causes the ions and electrons to drift out of the torus to larger major radii R. This is because when we bend the cylinder into a torus, we make the B field stronger on the inside of the torus than on the outside; this higher magnetic pressure on the inside pushes the plasma out of the torus. To prevent the ions and electrons from drifting out of the torus, we add a poloidal magnetic field; this allows the ions and electrons to drift along the B field lines, that are now helical, and shorts out the charge separation that made the electric field. The plasma is now confined in the torus. The poloidal field is the confining magnetic field in the torus; the toroidal field is used to provide stability.

The magnetic field lines doesn't always return to its starting point after a single rotation around the tokamak. The number of rotations it takes to return to the starting point depends on the strength of the poloidal magnetic field compared to the the strength of the toroidal magnetic field, as well as the circumference of the helical orbit. So at different minor radii in the plasma magnetic fields will make a different

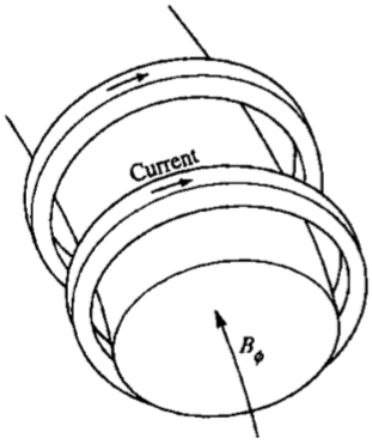

Figure I.2: The toroidal magnetic field B_ϕ is generated from coils that wrap around the tokamak like in this figure [1].

number of poloidal rotations with one toroidal rotation.

Rather than think of many helically orbiting magnetic fields on varying minor radii, it is easier to think about magnetic sheets on different minor radii. These magnetic sheets on different minor radii are magnetic flux surfaces. Flux surfaces are surfaces that enclose a constant amount of magnetic flux. We generally use poloidal flux surfaces, meaning enclosing constant amount of poloidal magnetic flux, the surfaces are contours of constant poloidal magnetic flux. Each flux surface has a value associated with its magnetic helicity known as the safety factor, q. So a safety factor of $q = 1$ would equate to a flux surface where in a single toroidal rotation the magnetic field is able to make a full poloidal rotation as well. q is called the safety factor because it is an indicator of the stability of the plasma. We often look at safety factor profiles to determine the quality of our simulation. The equation describing the safety factor is displayed in equation 2. The toroidal magnetic flux over the poloidal magnetic flux.

$$q = \frac{d\Phi}{d\Psi}[1] \tag{2}$$

A discussion on equilibrium can't be concluded without mentioning the Grad-Shafranov equation. The Grad-Shafranov equation is the constraining equation in all magnetohydrodynamics (MHD) equilibrium reconstruction codes. It starts with a simple assumption that the sum of the forces in the plasma is 0, or that the confining force of the magnetic field is equal to the expanding force of the pressure gradient $j \times B = \nabla p$. This is the volume current density cross the magnetic field should be equal and opposite to the derivative of the thermal pressure. To solve this equation for a tokamak we assume it is toroidally symmetric, this leads to the Grad-Shafranov

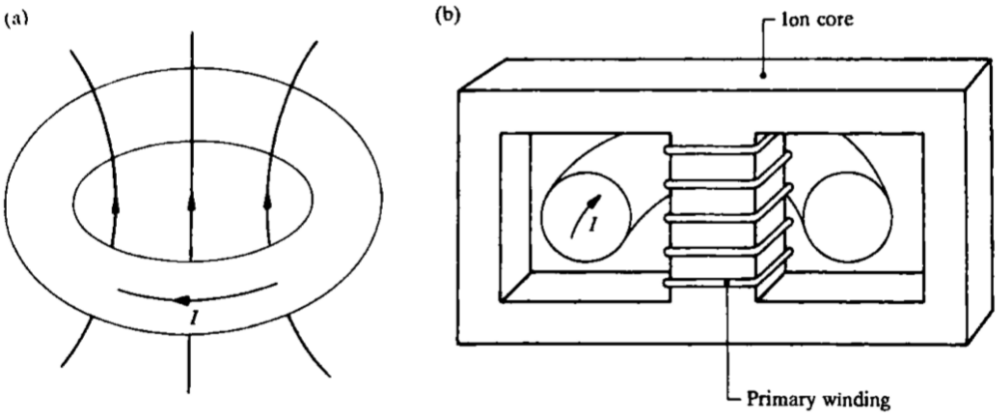

Figure I.3: The plasma current is created by the primary winding that is in the center of the plasma. This is also the winding with the most current [1].

shown in equation 3.

$$R\frac{\partial}{\partial R}\frac{1}{R}\frac{\partial \Psi}{\partial R}+\frac{\partial^2 \Psi}{\partial z^2}=-\mu_0 R^2 p'(\Psi)-\mu_0^2 f(\Psi)f'(\Psi)[1] \tag{3}$$

R is the major radius, Ψ is poloidal flux, z is the height and is orthogonal to the major radius, μ_0 is the vacuum permeability, and f is the poloidal current density. When equation 3 is plotted at a single toroidal angle it produces the equilibrium shown below in figure I.5. Notice the Grad-Shafranov equation describes the family of toroidally symmetric plasma equilibria; EFIT is a computer code that solves the equation for a specific set constraints provided by magnetic probes and pressure profile measurements.

I.2.3 EFIT and Kinetic EFIT

EFIT and Kinetic EFIT, are 2-Dimensional equilibrium reconstruction codes used by DIII-D. The codes use diagnostic information from inside the tokamak to calculate specific solutions from the Grad-Shafranov equations. This creates an equilibrium similar to the one displayed in figure I.5. EFIT is a magnetics only equilibrium reconstruction, it calculates flux surfaces iteratively by varying the current and pressure profiles to find solutions to the Grad-Shafranov equation, equation 3, which it then tests against magnetics data. EFIT denotes an equilibrium reconstruction that is 65 by 65 resolution, as explained in section II.1, we used EFIT code at a higher resolution. EFIT is usually implemented during a run at DIII-D to get real-time read out of the plasmas flux surfaces because its reconstruction is very fast. However, this assumes that the pressure and current profiles are completely represented by the magnetics data [7].

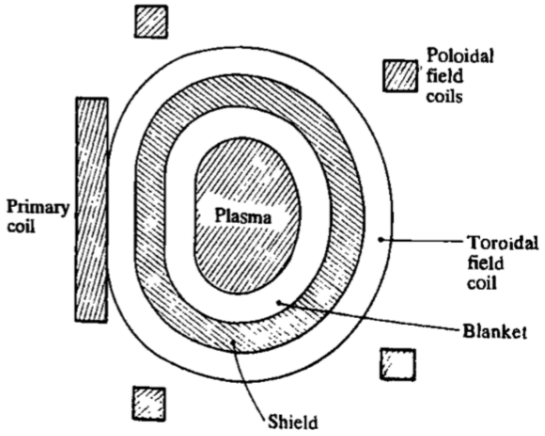

Figure I.4: This is a standard tokamak cross-section. A toroidal slice of the right side of the tokamak; if the tokamak were to keep going it would wrap around to the left and back on itself [1].

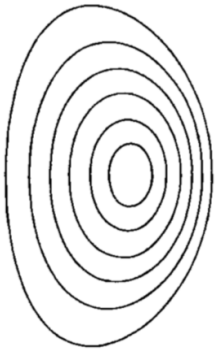

Figure I.5: Magnetic Flux Surfaces [1]

Kinetics EFIT takes into account the internal current and kinetic profile measurements. The internal current is calculated in DIII-D using the Motional Stark Effect, or MSE, diagnostics to measure the local pitch angle of magnetic field lines within the plasma [7]. The kinetic pressure profile data is given by density and temperature measurements made by the electron cyclotron emission (ECE), Thomson scattering (TS), and charge exchange recombination (CER) diagnostics [7]. Kinetic EFIT is a full MHD equilibrium reconstruction that takes into account magnetics data, MSE, and kinetic profile measurements when solving the Grad-Shafranov equation, equation 3.

I.2.4 H-mode and L-mode

Everything mentioned previously is a theoretical conception of tokamaks. Current tokamaks, such as DIII-D, run plasma in H-mode. H-mode is a plasma regime

that was achieved by accident with neutral beam heating experiments on ASDEX [1]. Previously tokamaks would run in L-mode, or low confinement, and have much lower confinement times. The poor confinement in L-mode is due to an increase in turbulence as the plasma is heated; this turbulence transports plasma across the confining magnetic field leading to decreasing confinement as more heating is added (this is what L mode is). Once a certain heating threshold is reached the plasma enters H-mode, or high confinement, which doubles the confinement time by increasing the edge confinement and suppressing turbulence. The plasma pressure and density on the edge increases, causing a rise in the density of the whole plasma. This increase in edge density is do to the flow rate on the edge [1]. An increase in flow shear on the edge of the plasma suppresses the instabilities. The change in flow rate on the edge also changes the plasma current on the edge, the bootstrap current. This increased pressure gradient near the edge, or pedestal pressure, causes a decrease in transport.

As the ∇p increases and broadens in the edge, the plasma reaches an instability threshold for a class of ideal MHD instabilities known as coupled peeling (current driven kink modes) and ballooning (resistive ballooning modes) that cause ELMs. Because the ELM results in a burst of plasma stored energy and pressure that is blown out into the boundary toward the wall the high pressure gradient in the H-mode edge relaxes, the sheared flow is damped out, and the turbulence increases again until it reaches the point where the plasma again spontaneously self-organizes into the sheared flow state with a large edge pressure gradient and suppressed turbulent transport. In this way, ELMs are a repetitive, cyclic instability. The issue is the short timescale on which the plasma stored energy is released leading to erosion and/or melting of the first wall/divertor of the device. The presence of ELMs decrease the H-mode efficiency unless contained; further explanation of this is in section I.2.6. There are also other special confinement modes such as V-H-mode and Q-H-mode that are interesting because they don't cause ELMs, but they either run into other stability limits or allow transport in another fashion.

I.2.5 Instabilities and Transport

Instabilities in MHD plasmas come from current and pressure gradients. There are two types of instabilities ideal modes and resistive modes. Ideal MHD modes have the name because the instability would still occur even if the plasma was a perfect conductor, while resistive modes depend on the resistivity of the plasma [1]. To describe these modes we use the variables m and n, poloidal and toroidal mode numbers respectively. These mode numbers can relate to the safety factor (2) by equation 4. A certain instability has a frequency which is described by the poloidal or toroidal mode number depending on the instability's symmetry. The toroidal magnetic field is very strong, and because of this it takes a good deal of energy to deform the magnetic field lines, which is what a mode or instability must do. When

the helicity of the mode is different from the helicity of the magnetic field lines, the mode must make a large bending of the magnetic field lines because it takes a large amount of energy. But on a rational surface, a flux surface where the magnetic field lines wind an integer number of times around the torus in the poloidal direction for each transit toroidally, any instability that has the same helicity as the field lines on that surface has to do a minimum amount of bending of the field lines and they loose their stabilizing force on the mode.

$$q = \frac{m}{n}[1] \tag{4}$$

Inabilities usually come in ideal and resistive pairs; such as the kink instability and the tearing mode [1]. The kink mode is an ideal mode and it causes a kink on the magnetic surfaces. Its resistive partner, the tearing mode, tears and reconnects magnetic field lines, this is due to the plasmas finite resistivity. This is a process called magnetic reconnection and it is not fully understood. Both the kink and tearing mode are driven by toroidal current gradient [1]. These instabilities occur on resonant flux surfaces determined by their mode number because they are changing the magnetic topology. Resonant flux surfaces are flux surfaces that create a rational safety factor with the instabilities mode number. The instability has certain pitch and the flux surface with the same pitch angle become perturbed and stochastic. Tearing modes, in particular, create islands from the magnetic reconnection, but only on the resonant surfaces. An illustration is displayed in figure I.6.

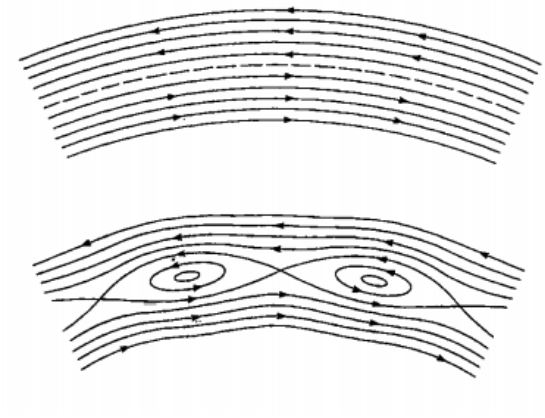

Figure I.6: Illustration of magnetic islands created from tearing modes [1].

These islands are important to the confinement of the plasma because the increase the diffusive transport of the tokamak. Diffusion coefficients take the form in all systems of a cross-system $step\ size^2/timescale$. For our plasma in a tokamak, this is a radial $step\ size^2/timescale$ and the characteristic diffusive step out of the system becomes not the very small radius of the gyration around the magnetic field, but is now the very large island width.

I.2.6 ELMS and RMPS

ELMs, or edge localized modes, are short bursts of plasma that leave confinement. ELMs have been found to be triggered by entering H-mode. These instabilities reduce temperature and density of the confined plasma, which lowers confinement, and can also damage the tokamak. ELMs come from a build up of temperature and pressure on a localized portion of the edge of the plasma and are found to be periodic [1]. There are 3 types of ELMs: type 1 ELMs are also called giant ELMs because they cause a huge amount of particles to leave the plasma, type 2 ELMs are significantly smaller than type 1 ELMs and don't cause much loss of confinement, type 3 ELMs are the smallest ELMs but are much more frequent and significantly lower confinement [1]. Note that ELMs are a good demonstration of the key issue with tokamaks: H-mode is a self-organization into a high confinement regime by suppressing turbulent transport, but despite this improved confinement, the result is simply that the plasma evolves faster to an MHD stability limit; in this case the peeling-ballooning limit and the onset of ELMs. In L-mode, the turbulent transport is so high that the plasma never reaches a high enough pressure to exceed the stability limit. This illustrates that what's needed is to increase the stability limits and/or to maintain the plasma in a steady state below the stability limit.

To mitigate ELMs DIII-D has implemented resonant magnetic perturbations, RMPs. RMPs are small magnetic perturbations, applied radially inward, to a resonant plasma flux surface. This increases transport, essentially slowly deflating the ELM instead of letting it burst. We believe this perturbation flattens the temperature and density gradient on the separatrix and leads to both magnetic islands and a stochastic region near the edge of the plasma, but have not confirmed this yet.

I.2.7 Divertor Strike Point Splitting

RMPs also cause the separatrix to oscillate in minor radius, this is because they are applied radially inward and can be described by a toroidal mode number. This oscillation in the separatrix causes a deformity in the stable and unstable manifold displayed in figure I.7, which usually lie on top of each-other. This stable and unstable manifold can grow large enough lobes that they intersect the lower region of the limiter. The lower region of the limiter, or divertor, is where the end of the separatrix magnetic flux surface hits in our configuration. The end of the separatrix is known as the strike point and the strike point splits when lobes of the stable and unstable manifold intersect the limiter, essentially allowing particles to be deposited at other locations than the strike point, or strike point splitting. We can image and model these deposited particles, or footprints, which occur when the lobes intersect the divertor during RMP ELM suppression. The goal is to accurately model these footprints to make predictions on which perturbation modes, $n =?$, better spread heat flux.

The boundary in figure I.7 is an illustration of the limiter. The region in the left

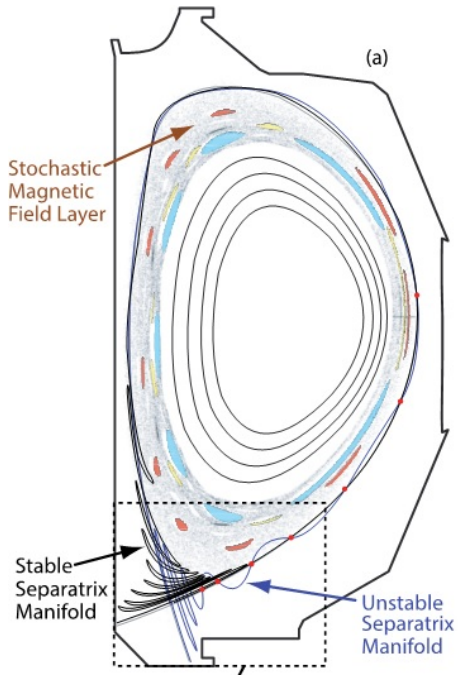

Figure I.7: Illustration of poloidal cross-section of plasma in DIII-D with RMP coils turned on [2].

side of the divertor region is the inner divertor. The footprint modeling and data is calculated and measured for the inner divertor of DIII-D. The strategy to spread heat flux and vary the footprints is to ramp the RMP's mode number from n = 2 to n = 3. This RMP ramp technique will hopefully shift the footprint pattern and spread the heat flux. The main purpose for the modeling is to see if it matches the data coming from DIII-D. We also want to know how sensitive the modeled splitting is to details of the equilibrium reconstruction so we can apply the same model on ITER's equilibrium conditions confidently.

II Methods

II.1 Equilibrium Reconstruction

How sensitive is the calculated splitting in the plasma response and vacuum models to details of the equilibrium reconstruction used? The equilibrium reconstructions is a 2D solution of the force balance (3) in the tokamak. There are varying types of equilibrium reconstructions utilizing varying degrees of precision in describing the equilibrium, such as inclusion of the H-mode pressure pedestal and bootstrap current just inside the separatrix. These equilibria also heavily constrain themselves using data from experiments and are used as a consistent starting point to compare

a simulation to actual data. The divertor footprints are modeled using two types of equilibria, magnetics only equilibria and kinetic equilibria. The grid resolution for these equilibria is 129 by 129. Figure II.1 below shows this poloidal cross-section. The

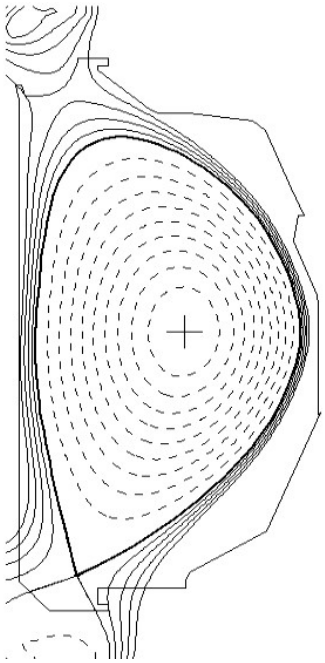

Figure II.1: Magnetics Only Equilibrium for shot 166439 at 3000 ms

difference between magnetics only and kinetic equilibria is how they model edge of the plasma and the very center of the plasma. The kinetic equilibria have a restriction keeping all the flux surfaces above $q = 1$. This is because kinetic equilibria are used for plasma response modeling and the MHD (Magnetohydrodynamics) code enlarges the $n = 1$ perturbation to levels not seen in the plasma itself. Kinetic equilibria also more accurately model the bootstrap current and pedestal pressure.

II.2 TRIP3D CPU and GPU Simulations

TRIP3D uses these equilibria to model how the magnetic field lines in the plasma will move with simulated error fields, error field correction fields, and RMPs. There is a CPU version of the code that produces Poincaré plots shown in figure III.2 and a GPU version of the code that parallelizes the computation to produce footprints. The Poincaré plot is used to determine the dominant perturbations of a particular equilibrium and can also help determine if an equilibrium is calculated incorrectly. The footprint computation is done using GPUs because it requires many more field lines to produce a reasonable plot. The footprint simulations have 72,000 start points

at $\phi = 0$ all the way around poloidally near the edge of the plasma. This is to ensure that enough of the launched field lines leave the plasma and hit the divertor to adequately map out the magnetic field line footprint. TRIP3D produces an output file, labeled hit.out, containing the points where the field lines hit the divertor. The hit.out file also includes the magnetic field line length from the starting point to the divertor target, determined largely by the number of toroidal transits before the field line crosses the separatrix and strikes the divertor target, and the plot produced simulates the footprint images taken in the inner divertor region in the DIII-D tokamak. The simulated points are color coded depending on the length of the field line.

II.3 USCD Fast Camera Images

The footprint simulations are compared to Fast Camera images of the inner divertor of DIII-D. Fast visible imaging is used to monitor the particle flux footprints and infrared imaging is used to monitor the heat flux footprints on the inner divertor. The simulation corresponds to particle flux as it shows magnetic field lines and consequently charged particles hitting the divertor wall of the tokamak. The particle flux is measured in the visible spectrum from 590 to 610 nm of molecular deuterium (D_2) emission. This provides spatially localized emission near the target plates that allows the footprint structure to be resolved. The ISP, or the inner strike point, is the region highlighted blue at the bottom of the picture in figure II.2. This is where we are comparing the TRIP3D simulations to the fast camera images. The blue highlights specifically are lobes, they comprise an experimentally imaged footprint of molecular D_2 emission. We want to accurately model the lobe spacing, known as splitting, and shape.

Fast Camera images meant for analysis are captured while the tokamak is running. As figure II.2 shows the camera views right through the plasma to the floor of the tokamak. A single run by the tokamak, or a shot, can last for four to eight seconds. A time history of the divertor footprint is obtained from the movie of the visible emission by averaging the emission over a narrow 4^o toroidal angle to avoid artifacts that might occur at divertor tile edges (dark radial lines in the image in fig. II.2) since the tiles are 5^o wide. The lobe positions in the footprint are then compared to the lobe positions in the simulation at the same toroidal angle. This is the sum of my analysis.

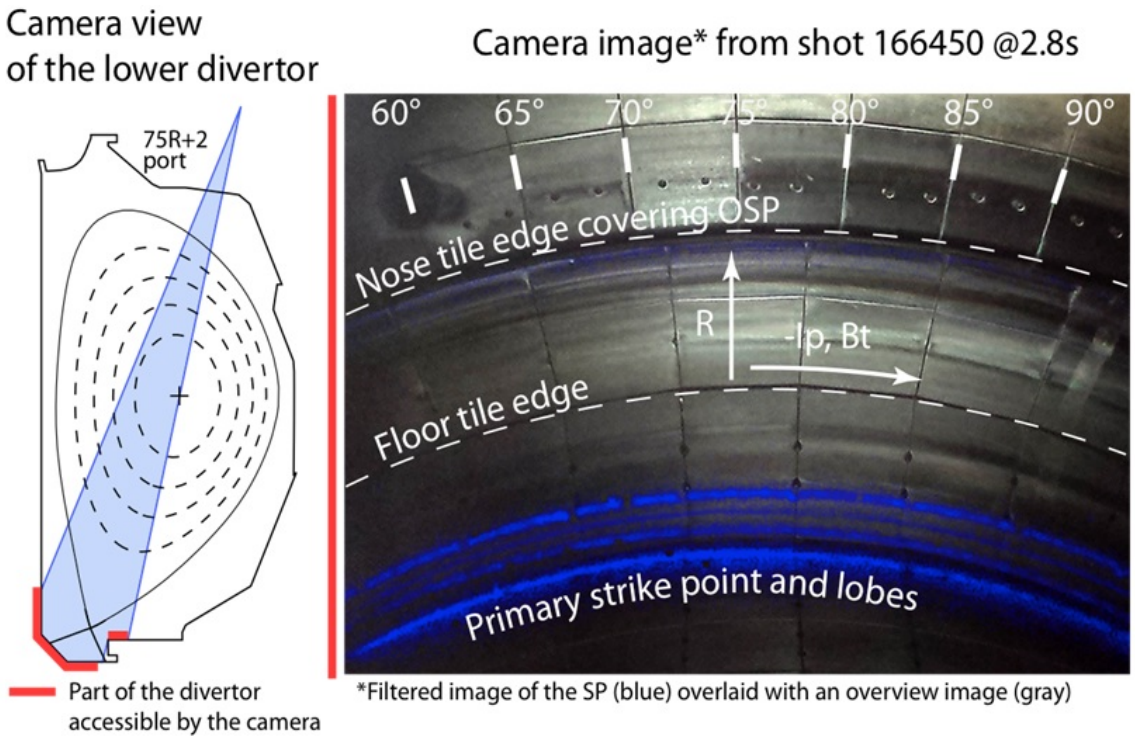

Figure II.2: Left- Illustration of Fast Camera view in DIII-D. Right - Fast Camera image of the divertor region in DIII-D. The blue bands in the bottom of the image are the measured molecular D_2 emission intensity, which is proportional to the D ion flux to the divertor target. Four distinct bands are readily visible instead of a single band in the absence of the RMP. [2].

III Results

III.1 Initial Queries on Simulated RMP Effects on Divertor Strike Point Structure

To make sure that the simulation is modeling the RMP effects correctly we can look at the Poincaré plot of the simulated plasma. A Poincaré plot displays where a magnetic field line intersects a certain toroidal angle, usually intersecting many times to give an idea of what is occurring to the magnetic field. A magnetic field line is followed around the torus. Each time the field line crosses the blue plane at a fixed toroidal angle, a "dot" is plotted to form the Poincaré plot. The diagram in figure III.1 is a good description of this process.

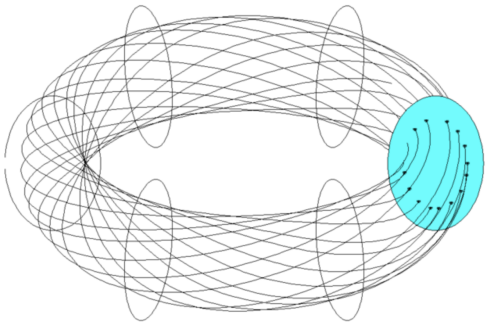

Figure III.1: Diagram of how a Poincaré plot is made for tokamaks [3].

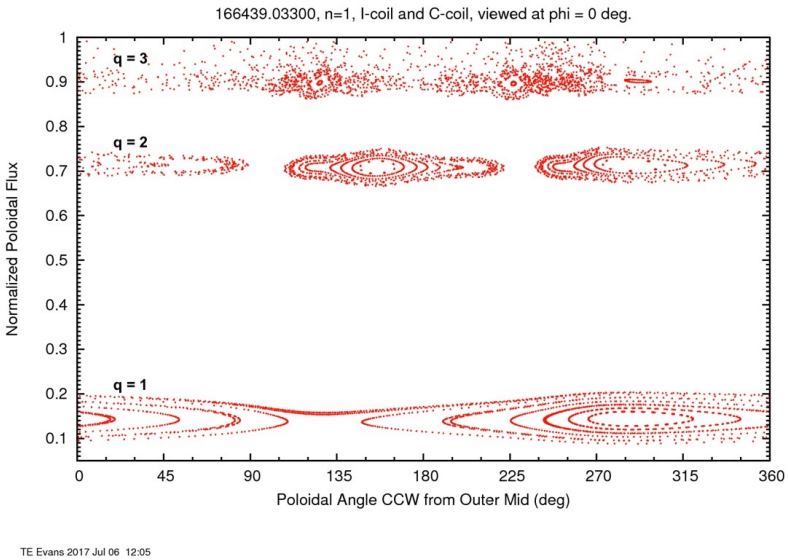

Figure III.2: Poincaré plot of TRIP3D modeled flux surfaces with Error Fields, Error Field Correction Fields(C-coil)

For the Poincaré plot in figure III.2, 0 on the y-axis corresponds to the center of the plasma. Normalized poloidal flux, or Ψ_n, is parallel to the minor radius, and is an effective radial coordinate that accurately represents the non-circular cross-section of the plasma equilibrium evident in the left side of figure II.2. The x-axis is the poloidal angle measured from the outboard mid-plane in the counterclockwise direction. The magnetic field lines were started at three radial locations the $q = 1$ surface, $q = 2$ surface, and $q = 3$ surface. The field lines were integrated around toroidally 200 rotations using TRIP3D.

Since $q = \frac{m}{n}$ [1], it is visible that the fields are mostly an $n = 1$ perturbation. On $q = 1$ surface there is 1 island, on the $q = 2$ there are 2 islands. Of course the islands aren't perfect which indicates there are other perturbations, but it is $n = 1$ dominated. On the $q = 3$ surface the field lines don't form a coherent shape, although three small magnetic islands are visible at poloidal angles of 128^o, 225^o, and 292^o. This surface is close to the separatrix and displaying stochastic effects [9]. This is a good confirmation that TRIP3D is modeling the magnetic effects correctly.

III.2 Equilibrium Uncertainty

To explain the footprint simulation results we need to first compare the equilibria. The different constraints we used to produce kinetic and magnetics only equilibria caused a dramatic shift in the main strike point and X-point shown in figure III.3. The X-point for the kinetic equilibrium clearly moves toward the center of the plasma. This gives the stable manifold more distance before it hits the divertor when TRIP3D is given a kinetic equilibria. This along with flux expansion should cause the TRIP3D runs with kinetic equilibria to have greater lobe splitting.

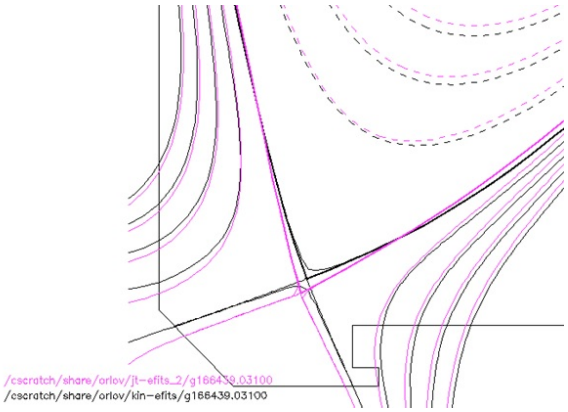

Figure III.3: Equilibrium comparison of shot 166439 at 3100ms with a kinetic equilibrium (black) and a magnetics only equilibrium(pink)

III.3 Footprints

The specific timeslice, for the TRIP3D footprint simulations, we will be looking at is 3100ms. Figures III.4 and III.5 display the footprint simulation run with magnetics only and kinetic equilibrium respectively. The blue region highlights where our Fast Camera would be taking data in DIII-D. The y-axis on the plots is the S-coordinate which is 0 at the center of the inner wall of the limiter and follows the wall poloidally in the counterclockwise. The x-axis is ϕ, the toroidal angle in the tokamak. The vertical dashed lines are respectively the toroidal angle of the IRTV that measures the heat flux (60^o) and the toroidal angle of the divertor floor Langmuir probe array (180^o). The horizontal black line is the transition from the 45^o tile (below the black line, $S < 1.22$) to the center post (above the black line, $S > 1.22$), as shown in figure II.2. The colors indicate the length of the magnetic field line from starting point (ψ_n, θ, ϕ) to the divertor target.

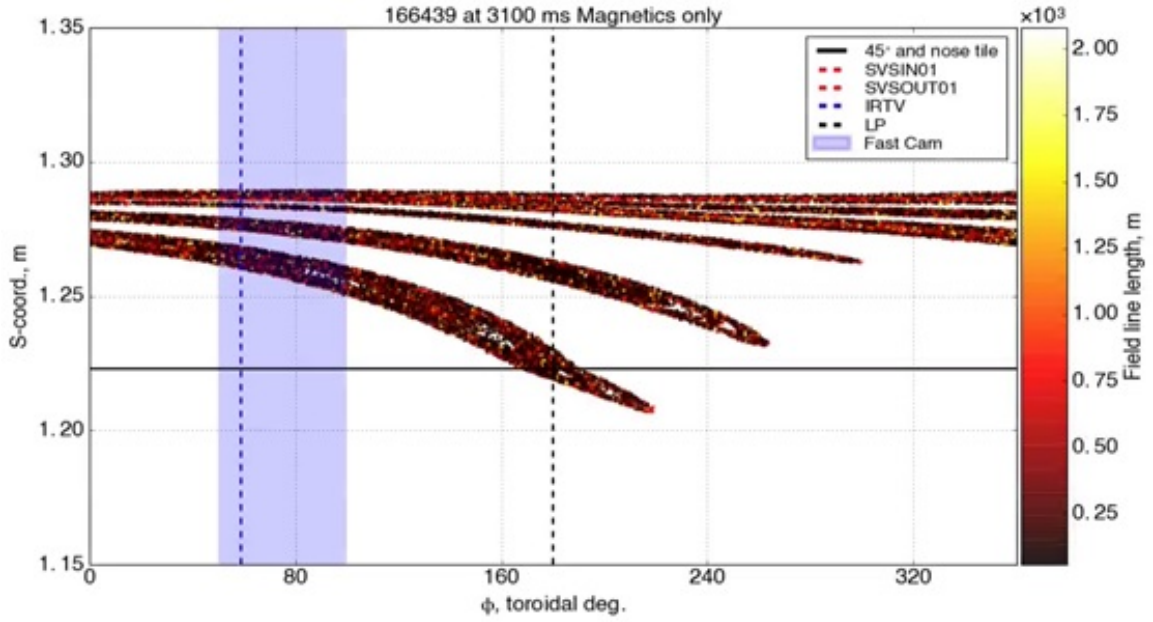

Figure III.4: TRIP3D simulated footprint of the inner divertor region with magnetics only equilibrium.

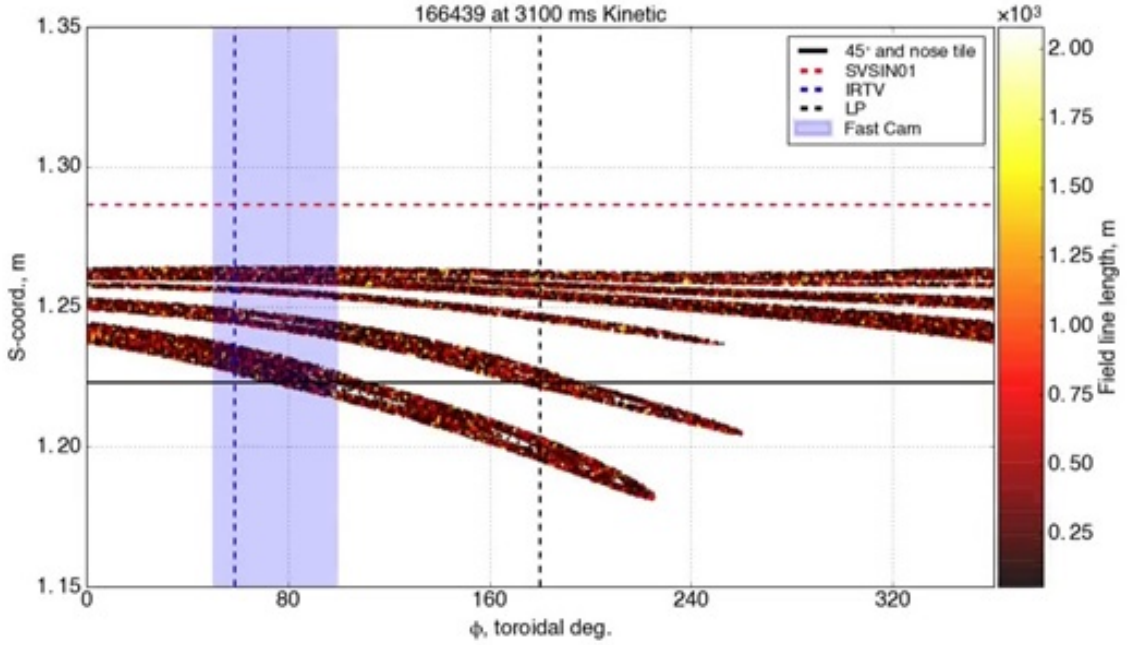

Figure III.5: TRIP3D simulated footprint of inner divertor region with kinetic equilibrium.

Notice the title of the modeled footprints. They are designed to easily identify the simulation parameters and follow that specific simulation through multiple types of plots. The title consists of the shot number, the time that has passed in the simulation for that shot in milliseconds, and the type of equilibrium used. All our simulations were done with a vacuum model so we don't need to differentiate between models using a kinetic equilibrium, which also occurs in plasma response. Also notice the legend which identifies many lines on the plots. The most important being SVSIN01. This is the equilibrium predicted strike point, it isn't noticeable in figure III.4 because the footprint simulation also predicts the same strike point, essentially covering the red dashed line. Figure III.5 shows a significant difference in this respect.

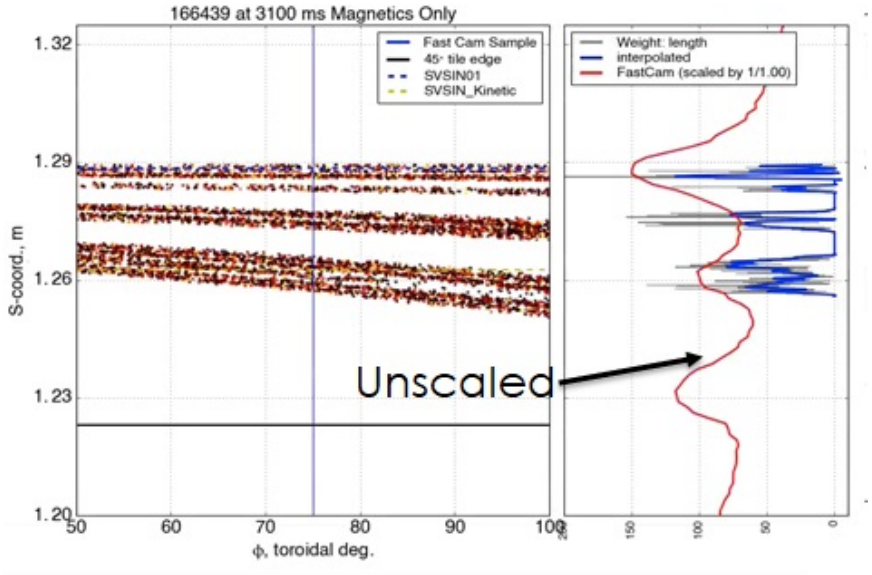

Figure III.6: Left - TRIP3D simulated footprint of inner divertor region with Magnetics Only equilibrium zoomed in to Fast Camera view. Right - Intensity plot of simulated magnetic field lines striking the inner divertor region (blue). Intensity plot of the measured D_2 emission in the inner divertor region of DIII-D (red).

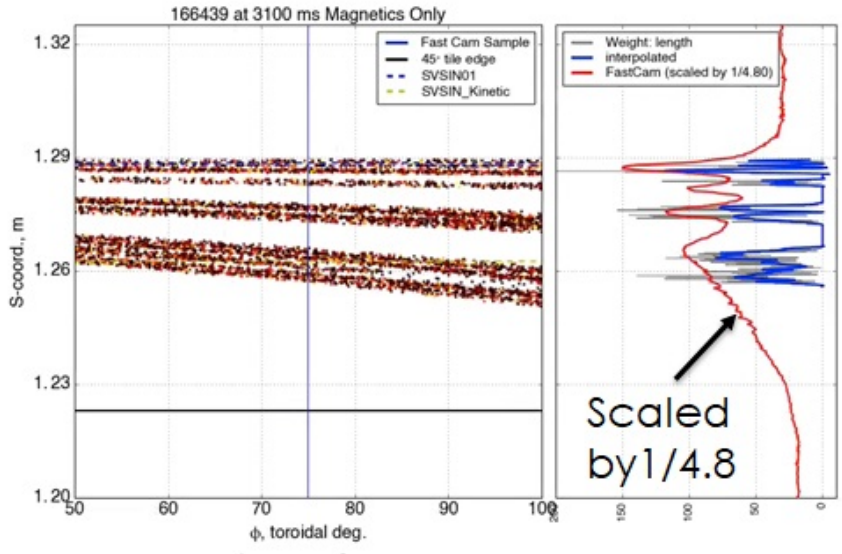

Figure III.7: Left - TRIP3D simulated footprint of inner divertor region with Magnetics Only equilibrium zoomed in to Fast Camera view. Right - Intensity plot of simulated magnetic field lines striking the inner divertor region (blue). Intensity plot of the measured D_2 emission in the inner divertor region of DIII-D (red), scaled down to fit simulated intensity plot.

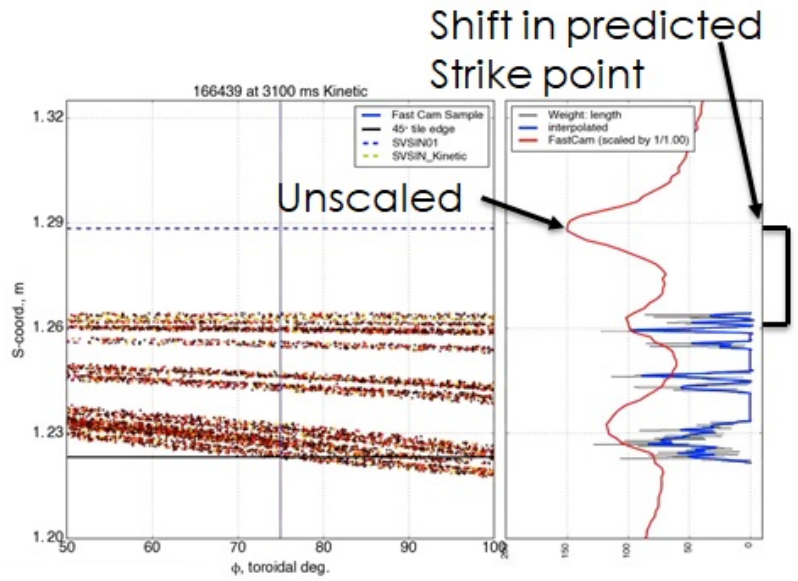

Figure III.8: Left - TRIP3D simulated footprint of inner divertor region with Kinetic equilibrium zoomed in to Fast Camera view. Right - Intensity plot of simulated magnetic field lines striking the inner divertor region (blue). Intensity plot of the measured D_2 emission in the inner divertor region of DIII-D (red).

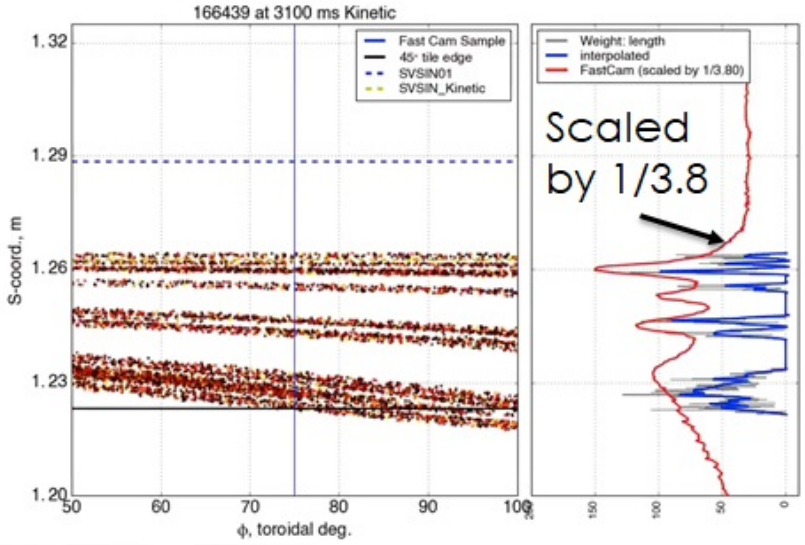

Figure III.9: Left - TRIP3D simulated footprint of inner divertor region with Kinetic equilibrium zoomed in to Fast Camera view. Right - Intensity plot of simulated magnetic field lines striking the inner divertor region (blue). Intensity plot of the measured D_2 emission in the inner divertor region of DIII-D (red), shifted and scaled to match simulated intensity plot.

The plots in figures III.6 to III.9 are comprised of two plots side by side that share the same y-coordinate. The left plot is TRIP3D footprint simulation at 3100ms, with the x-axis limited to a region only the Fast Camera can take data. The right plot is an intensity profile of the TRIP3D simulated footprint at $\phi = 75^o$ in blue and an intensity profile made from data taken by the Fast Camera at $\phi = 75^o$ in red. More specifically, the intensity profiles at 75^o are of the measured D_2 emission in DIII-D (the red profile) and field line density in the simulation (the blue profile). It is clear that the simulations predict much smaller splitting than the Fast Camera is measuring. Notice that the footprint simulation done with the kinetic equilibrium has a shifted strike point from the strike point in the Fast Camera data. The simulation done with the kinetic equilibrium also has larger splitting than the magnetics only case, demonstrating earlier prediction made from the differences in the equilibria X-point. These simulations were done for many time slices and we compare the intensity profile of all the time slices at 75^o in figures III.10 through III.14.

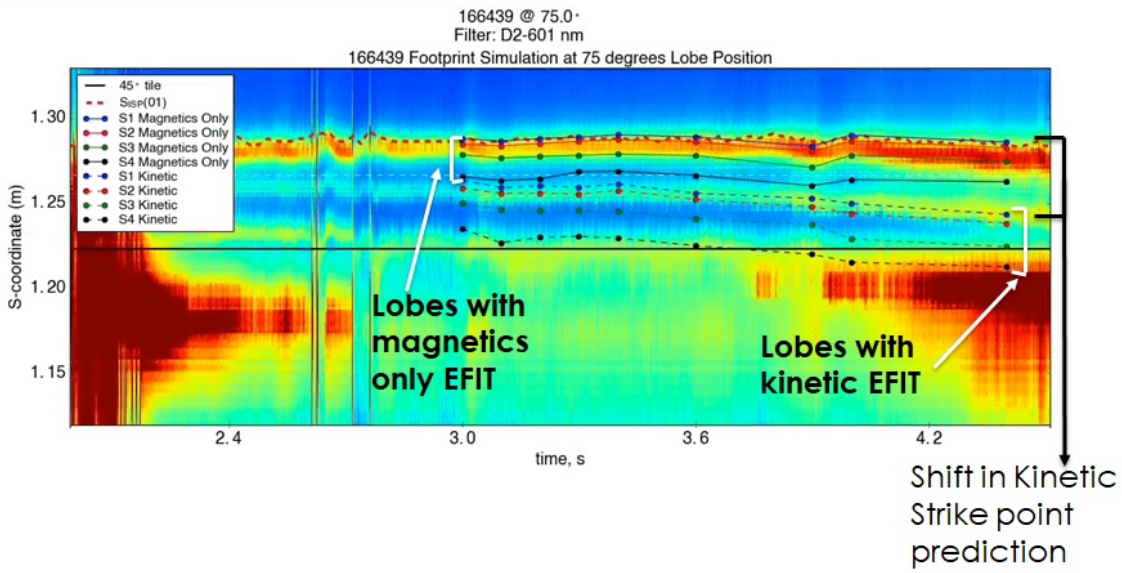

Figure III.10: Fast Camera imaging of D_2 emission of the inner divertor region at a single toroidal angle (75^o) from 2 to 4.5 seconds with simulated lobe positions from Magnetics Only (solid lines) and Kinetic (dashed lines) equilibrium overlaid.

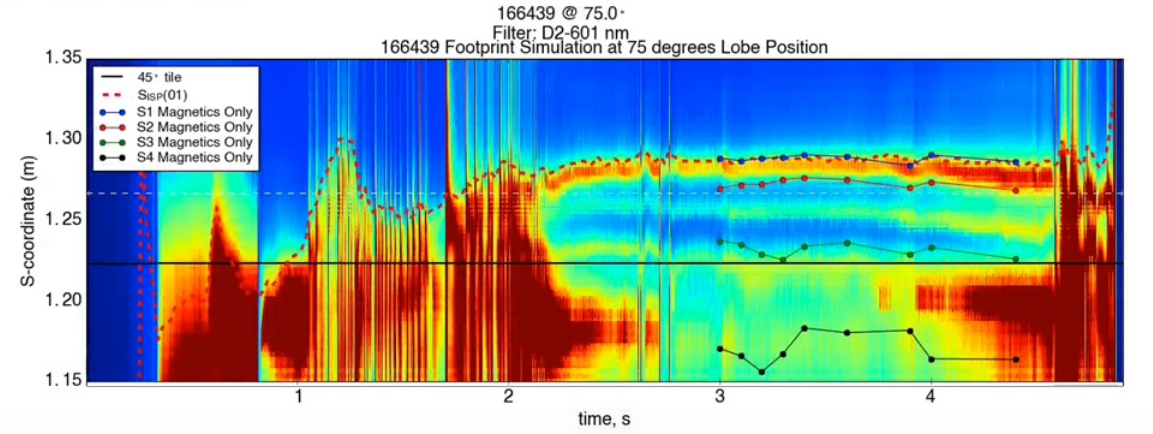

Figure III.11: Fast Camera imaging of D_2 emission of the inner divertor region at a single toroidal angle (75^o) from 0 to 5 seconds with simulated lobe positions from Magnetics Only equilibrium (solid lines) overlayed and simulated lobe positions scaled to fit Fast Camera data.

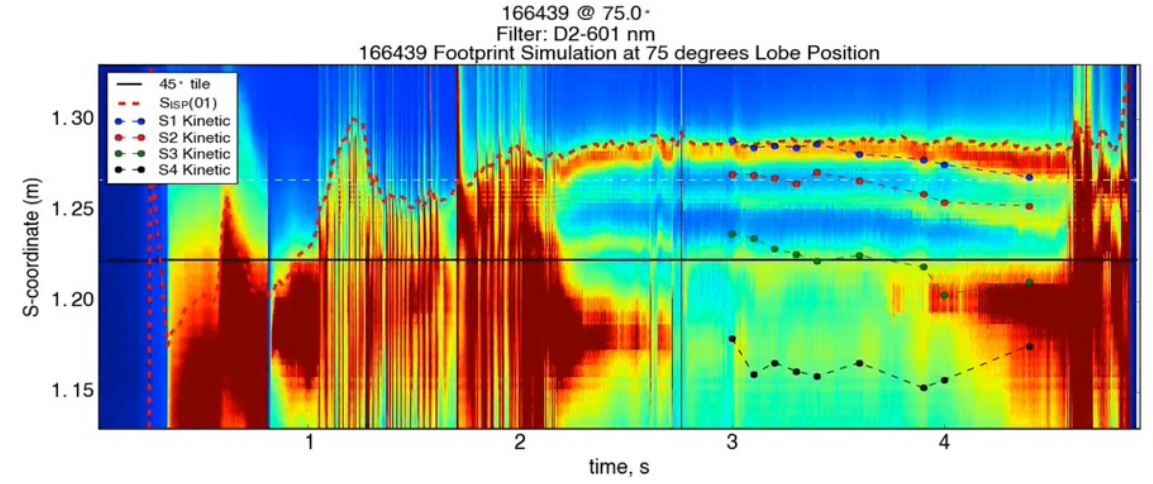

Figure III.12: Fast Camera imaging of D_2 emission of the inner divertor region at a single toroidal angle (75^o) from 0 to 5 seconds with simulated lobe positions from Kinetic equilibrium (solid lines) overlayed and simulated lobe positions scaled to fit Fast Camera data.

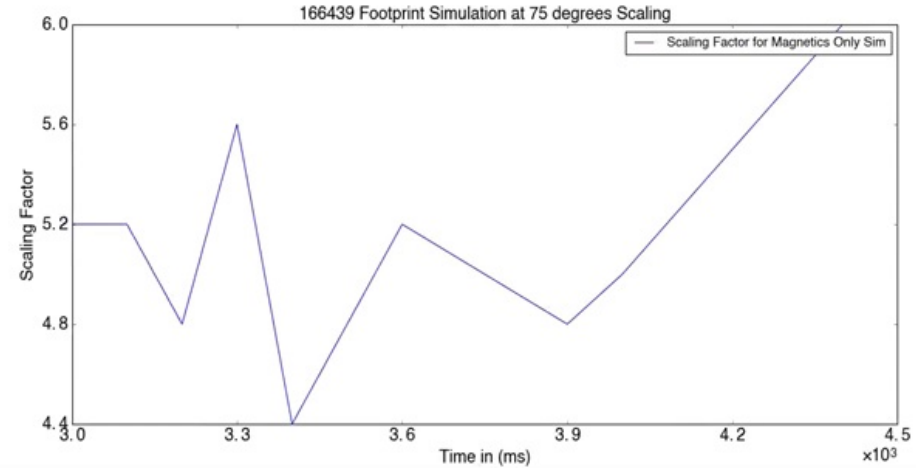

Figure III.13: Scaling of TRIP3D simulated lobe positions with Magnetics Only equilibrium at 75^o from 3 to 4.5 seconds.

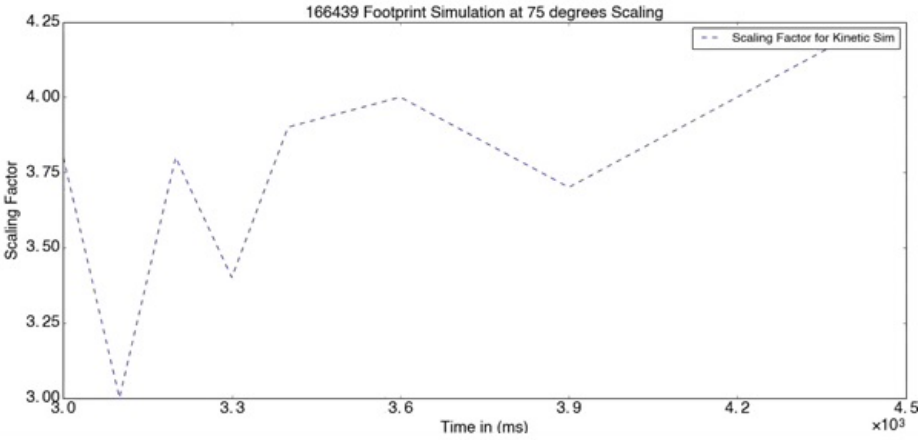

Figure III.14: Scaling of TRIP3D simulated lobe positions with Kinetic equilibrium at 75^o from 3 to 4.5 seconds.

It is important to note that in figure III.11 and figure III.12, the overlayed points had their splitting scaled time dependently. The scaling can be seen in figures III.13 and III.14. Figure III.11 and figure III.12 show the intensity of the D_2 emission, in DIII-D for shot 166439 at 75^o as a function of time. This data is displayed as a heatmap with the y-axis being the S-coordinate and the x-axis being time. The connected points overlaid on the image are TRIP3D simulated lobe positions corresponding to the 4 predicted lobes in the TRIP3D simulations. Figure III.10 has the Fast Camera data and the TRIP3D simulation done with both magnetics only and kinetic equilibria. Figure III.11 displays the Fast Camera data and a time dependently scaled TRIP3D simulation with a magnetics only equilibrium. Figure III.12 shows the Fast Camera data and a time dependently scaled TRIP3D simulation with a kinetic equilibrium. Notice that the simulation with a magnetics only equilibrium had a more difficult time fitting to the Fast Camera data, while the simulation with a kinetic equilibrium tend to fit the Fast Camera data better, especially at later time slices.

IV Discussion

IV.1 Equilibrium Uncertainty

The difference in the X-point comes from a difference in plasma current between the two equilibria. For the equilibrium in figure III.3 the difference is 12.1 kA, when the total plasma current is near 1.5 MA. This is enough to cause a 3 cm shift in the main strike point. This is reflected in the subsequent footprint simulations using kinetic equilibria. As the simulations will show the magnetics only simulations more accurately predict the main strike point when compared to the camera data. The simulations we have currently run are vacuum simulations. When we get to plasma response simulations this issue will only be magnified because of the MHD code, in our case M3D-C1, will again shift the strike point. This has to do with how M3D-C1 calculates the force balance in the plasma. Kinetic equilibrium have a uniform grid, but MHD codes need an adaptive grid with higher resolution around resonant flux surfaces. This difference in resolution causes M3D-C1 to recalculate the force balance on its native grid to ensure adequate convergence to a force free equilibrium. It doesn't interpolate because that would cause convergence errors, and because M3D-C1 doesn't have the full capabilities of EFIT to match experimental data, the recalculation causes shifts in the strike points and X-point. Of course people are finding ways around this problem like varying currents in a limited number of coils to make the M3D-C1 equilibrium match the kinetic EFIT it was given. Figure IV.1 is an example of this issue.

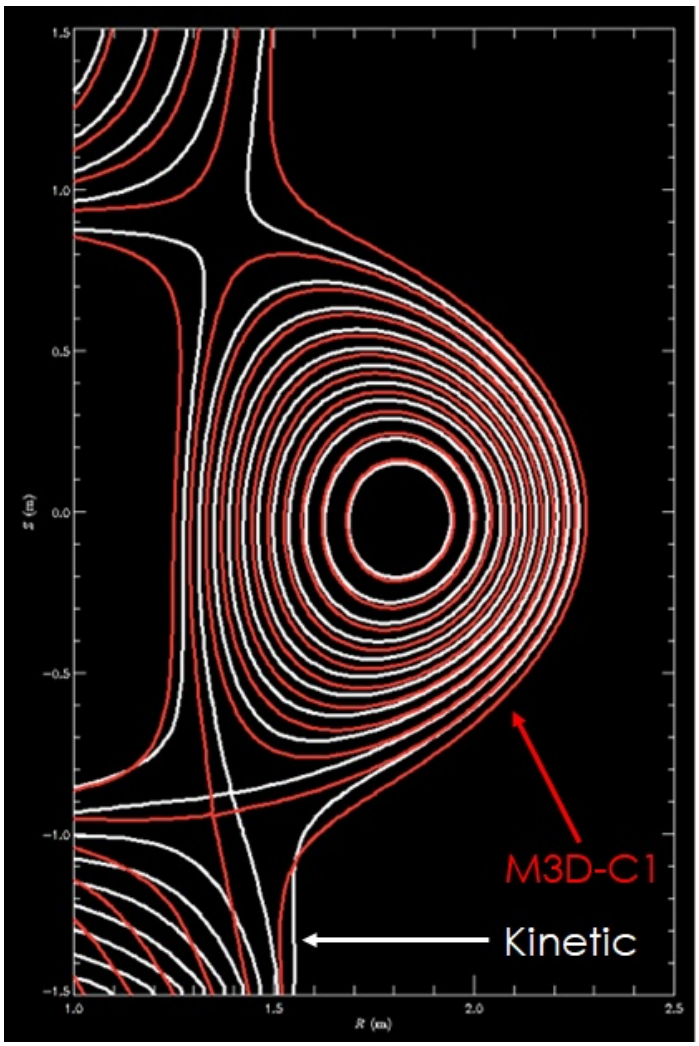

Figure IV.1: Example Equilibrium from K-STAR facility in South Korea for (white) a kinetic equilibrium calculated with EFIT, and (red) the equilibrium recomputed by M3D-C1 on its native grid without the experimental constraints used by EFIT.

IV.2 Footprints

The TRIP3D simulated footprints, or vacuum modeled footprints, under-predicts the lobe splitting by approximately a factor of 5. This is seen in figures III.13 and III.14, but is more obvious in figures III.6 and III.8. The difference lobe splitting between the simulation and the Fast Camera data is a persistent problem. The scaling factor is sensitive to the equilibrium and is time dependent. It is not yet known if the scaling factor is sensitive to the toroidal angle because all the intensity analysis was done at $\phi = 75^o$. However, this sensitivity could be due to a lack of precision and transitioning to a plasma response model, from our current vacuum model, could lower the sensitivity of the scaling.

Also, kinetic equilibria predict the lobe splitting to be larger than its magnetics only counter part, resulting in a smaller scale factor with the kinetic equilibria as shown in figure III.14. However, this is most likely due to the difference in constraints between the two equilibria and most likely has no bearing on kinetic equilibria accuracy. The most probable answer being the X-point distance growing in the kinetic equilibrium's case, giving the lobes more time to separate before hitting the limiter. This difference in constraint between the kinetic and magnetics only equilibria also causes a noticeable shift in the main strike point. The main cause being the difference in plasma current. Magnetics only equilibria with matching constraints to the kinetic equilibria, or kinetic equilibria with the strike point constrained are being made. Hopefully they will bring a more straight forward comparison of footprint simulations.

Lastly, the footprint simulation with a kinetic equilibrium fits the Fast Camera data better than the magnetics only simulation, in terms of time dependent trends. The difference in fit can be seen by comparing figure III.12 to figure III.11. This is surprising considering the initial issues we had with the kinetic equilibria. However, considering that the kinetic equilibria have more experimental constraints it would make sense that the simulations done with the kinetic equilibria fit the data better. Of course new kinetic equilibria that have a constrained strike point or X-point will have to be made and used to simulate the same shot and timeslice to make sure that the fit holds.

V Conclusion

The most important result from our simulations is the consistent need for a scaling factor for vacuum models using both magnetics only and kinetic equilibria. Previously, footprints modeled with kinetic equilibria were not analyzed this way. Also very significant is the the need for time dependent scaling for the TRIP3D simulation to fit the measured splitting. TRIP3D simulated lobe positions over time is a

completely new form of analysis that has given us more confidence is the vacuum models done with kinetic equilibria; equilibria constraints aside. Why there is such a difference in the measured and simulated splitting is still an issue to be considered. We know the TRIP3D is simulating the flux surfaces response to the RMPs correctly because of the Poincaré plots, yet the splitting is off by a factor of 5. Moving from a vacuum model to a plasma response model is the first thought to resolve this issue, but it is not clear why a plasma response model would because intuition indicates the splitting would be smaller in a plasma response model.

There is not full confidence in the footprint simulations yet. The goal was to show significant agreement among different simulations and low sensitivity to equilibrium uncertainty, so that a simulation of the RMP ramp technique applied to ITER conditions - that displayed significant heat distribution in the divertor region - is considered a viable result. The TRIP3D footprints display relative agreement, but have an overall scaling issue. There are still more steps needed to get to a viable results of significant heat distribution in ITER.

References

[1] J. Wesson, *Tokamaks*, 3rd ed. Oxford University Press, 2004.

[2] R. Moyer, I. Bykov, D. Orlov, J. Lee, T. Evans, R. Nazikian, M. Makowski, C. Lasnier, H. Wang, T. Abrams *et al.*, "Imaging divertor strike point splitting in rmp elm suppression experiments," in *58th Annual APS Meeting*, ser. Division of Plasma Physics, San Jose, California, 2016.

[3] "Poincaré plot diagram," 2018. [Online]. Available: https://computation.llnl.gov/projects/starsapphire-data-driven-modeling-analysis/poincar%C3%A9-plots

[4] T. Evans, D. Orlov, A. Wingen, W. Wu, A. Loarte, T. Casper, O. Schmitz, G. Saibene, M. Schaffer, and E. Daly, "3d vacuum magnetic field modelling of the iter elm control coil during standard operating scenarios," *Nuclear Fusion*, vol. 53, no. 9, p. 093029, 2013.

[5] T. E. Evans, R. A. Moyer, K. H. Burrell, M. E. Fenstermacher, I. Joseph, A. W. Leonard, T. H. Osborne, G. D. Porter, M. J. Schaffer, P. B. Snyder *et al.*, "Edge stability and transport control with resonant magnetic perturbations in collisionless tokamak plasmas," *nature physics*, vol. 2, no. 6, pp. 419–423, 2006.

[6] C. Wong, S. Malang, S. Nishio, R. Raffray, and A. Sagara, "Advanced high performance solid wall blanket concepts," *Fusion engineering and design*, vol. 61, pp. 283–293, 2002.

[7] L. Lao, H. S. John, Q. Peng, J. Ferron, E. Strait, T. Taylor, W. Meyer, C. Zhang, and K. You, "Mhd equilibrium reconstruction in the diii-d tokamak," *Fusion science and technology*, vol. 48, no. 2, pp. 968–977, 2005.

[8] R. Fitzpatrick, "Effect of nonlinear energy transport on neoclassical tearing mode stability in tokamak plasmas," *Physics of Plasmas*, vol. 24, no. 5, p. 052504, 2017.

[9] T. Evans, R. Moyer, and P. Monat, "Modeling of stochastic magnetic flux loss from the edge of a poloidally diverted tokamak," *Physics of Plasmas*, vol. 9, no. 12, pp. 4957–4967, 2002.